Turbo Equalization with Convolutional and LDPC Codes as well as Analytically Computed Metrics

Tobias Rankl
University of Stuttgart, Institute for Telecommunications, 70569 Stuttgart
E-mail: tobias.rankl@inue.uni-stuttgart.de

Abstract

This paper compares advanced electrical equalization schemes for intensity modulated high speed fiber optic transmission. The treated equalization schemes are based on the Turbo principle and apply convolutional as well as low-density parity-check (LDPC) codes with a forward error correction (FEC) overhead of 6.7%. A bit error rate (BER) and EXIT chart analysis based on a sophisticated channel model and analytically computed branch metrics for the BCJR and Viterbi equalizers give detailed insight into the performance and into the iterative equalization process, respectively.

1 Introduction

Electrical equalization, detection and decoding circuits for high speed fiber optic communication lines are effective and economic solutions to improve the signal quality at the receiver site. In recent years a variety of algorithms where investigated in oder to match the general conditions in fiber optic communications [1]. Viterbi equalizers [2], feed forward and decision feedback equalizers [3]–[5], as well as a large number of different forward error correction (FEC) schemes [6]–[8] where studied by many researchers. A combined approach of equalization and decoding is Turbo equalization [9]. With this method a feedback loop from decoder output to the equalizer is introduced. This technique can outperform almost any other receiver scheme of comparable or lower complexity, by far.

In this paper we compare two basic Turbo equalization schemes which came recently into the focus of the research community. The first is Turbo equalization based on convolutional codes [9], the second is Turbo equalization based on low-density parity-check (LDPC) codes [10]. Both approaches are similar to each other and consist of a Bahl-Cocke-Jelinek-Raviv (BCJR) [11] maximum a posteriori (MAP) soft-in soft-out (SISO) detector as well as of an MAP SISO decoder for the FEC codes.

Due to the ability to decode LDPC codes iteratively, two different parameter settings (with and without LDPC decoder iterations) are applied to the LDPC coded Turbo equalizer. The performance of both methods is investigated and compared to the Turbo equalizer with the convolutional code as well as to some standard receiver schemes (e.g. Viterbi equalizer with Reed-Solomon (RS) code of type RS(255,239) or a threshold detector and RS(255,239) decoder [12]).

The project is supported by the German research foundation (Deutsche Forschungsgemeinschaft, DFG)

The branch metrics which are necessary for the trellis based BCJR and Viterbi detection are computed by use of an analytical computation method that is based on a Karhunen-Loève series expansion as well as on a moment generating function calculus [13].

The paper is organized as follows. Section 2 introduces the Turbo equalizers. Section 3 describes the applied model of the fiber optic transmission link and outlines the mathematical background of the analytical branch metric computation. In section 4 BER and EXIT chart [14] are discussed and deeper insights into the iterative equalization processes of the Turbo equalizers are given. In section 5 conclusions are given.

2 The Turbo Equalizers

In this section the basic concept of Turbo equalization is introduced. Further the three Turbo transmission schemes under study are described and some details on the applied FEC codes are given.

A Turbo equalizer consists in general of a concatenation of two encoding components that are iteratively decoded. The two elements are called outer and inner code component. In the case at hand the outer component is the FEC code, the inner component is the communication channel which is eventually combined with a binary recursive convolutional encoder, which is called precoder [9]. As mentioned, this paper compares a convolutional coded Turbo equalizer to two different LDPC coded Turbo equalizers. These three types of equalizers are shown in Figs. 1 (a) to (c) and are investigated in this paper. They are explained in the following.

Type (a) receiver: A simple concatenation of BCJR equalizer and iterative LDPC decoder. No precoder is used in this case (the reason is shown in section 4). The

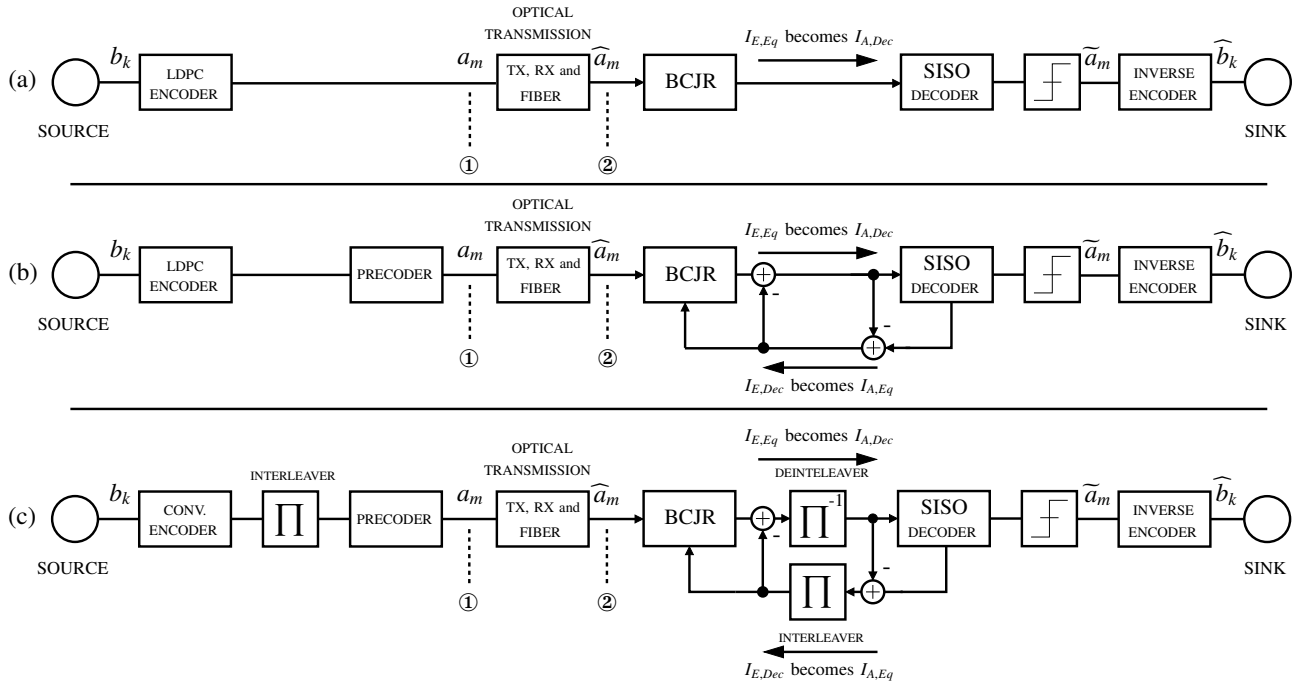

Fig. 1. Block diagrams of Turbo equalizers. (a) LDPC coded equalizer with LDPC decoder iterations and (b) LDPC coded Turbo equalizer. (c) Turbo equalizer with convolutional codes.

number of LDPC decoder iterations is 25. This type of receiver is a complexity reduced receiver of type (b), it does not perform Turbo equalization iterations.

Type (b) receiver: LDPC coded Turbo equalizer with precoder and only a single LDPC decoder pass. 25 Turbo equalizer iterations are performed.

Type (c) receiver: Convolutional coded Turbo equalizer with precoder and 25 Turbo equalizer iterations. Since the convolutional encoder as well as the fiber channel correlate adjacent bits the interleavers are necessary in order to separate both code elements (FEC code and fiber channel) information theoretically. Because of the different structure of LDPC codes, the interleaver is not necessary for the LDPC coded Turbo equalizers.

The applied convolutional code is a punctured $R_c = n/(n+1)$ (with $n = 15$) memory 3 recursive code with forward polynomial $G = 013$ and recursive polynomial $G_r = 015$, the code word length is $N = 65550$ [9]. As decoder a BCJR algorithm is used. The LDPC code is a quasi cyclic Euclidean geometry code [15] of type 1 with parameters $m = 2$ and $s = 6$ the code is 16 times column extended and of code word length $N = 65550$. As decoder the sum product algorithm (SPA) [15] either with or without iterations is used. The code rate of both, convolutional code and LDPC code is $R_c = 6.7\%$, the code length of $N = 65550$ is about half of the size of an OTU-3 frame [16].

The optical transmission channel with transmitter (TX), fiber and optically preamplified receiver (RX) in Fig. 1 is modeled as shown in Fig. 2. The section ① – ② in Fig. 1 is outlined in Fig. 2(a,b).

3 System Model and Analytical Branch Metric Computation

In this section the signal transmission over the optical fiber including optical transmitter and preamplified optical receiver is introduced. Fig. 2(a) shows the system model. The analytical computation of the branch metrics for BCJR and Viterbi equalizer is also outlined in this section.

3.1 The System Model

The transmission system which is depicted in Fig. 2(a) consists of a transmitter with the electrical preprocessing, which contains the FEC encoder and eventually the precoder. Further is consists of a standard singe mode fiber (SSMF) and of a preamplified optical receiver [17] which is followed by the concatenation of equalizer and decoder. The corresponding lowpass equivalent is shown in Fig. 2(b). The signals in this Figure will mathematically described in the following.

$\overrightarrow{s(t)}$ at the TX output can be written as

$$\overrightarrow{s(t)} = \vec{e}\sqrt{\sum_{m=-\infty}^{\infty} a'_m P_{cw} g\,(t - mT_s)}, \qquad (1)$$

where $\overrightarrow{s(t)} = [s_x(t), s_y(t)]^T$. It represents the linear polarized plane optical wave that is launched into the transmission fiber. $\vec{e} = [\cos\alpha_{pol}, \sin\alpha_{pol}]^T$ is the polarization Jones vector and α_{pol} is the angle deflection of

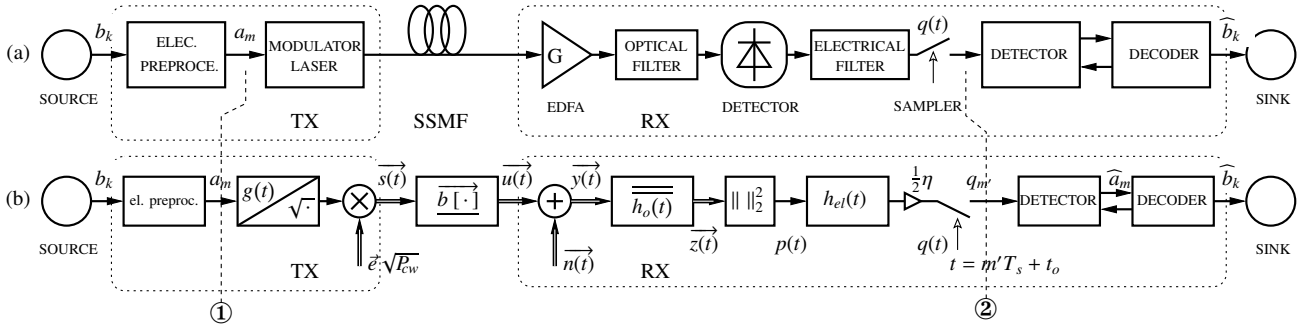

Fig. 2. Fiber optic transmission line with transmitter (TX), standard singe mode fiber (SSMF) and optically preamplified receiver (RX). (a) System model of the optical communication line, (b) Lowpass equivalent model.

the linear polarization with respect to the x-polarization. a'_m is the binary data sequence that already contains the influence of the signal extinction ratio γ, P_{cw} is the power of a continuous wave laser and $g(t)$ is the impulse response of the impulse shaper. Chirp free linear intensity modulation is performed by an electro absorption modulator.

The propagation of the transmit signal in the optical fiber can be described by a pair of nonlinearly coupled nonlinear Schrödinger equations [18]. These equations are

$$\frac{\partial a_x}{\partial z} + \beta_{1x}\frac{\partial a_x}{\partial t} + \frac{j}{2}\beta_{2x}\frac{\partial^2 a_x}{\partial t^2} + \frac{\alpha_{loss}}{2}a_x = j\gamma_{nl}\left(|a_x|^2 + \frac{2}{3}|a_y|^2\right)a_x \tag{2}$$

$$\frac{\partial a_y}{\partial z} + \beta_{1y}\frac{\partial a_y}{\partial t} + \frac{j}{2}\beta_{2y}\frac{\partial^2 a_y}{\partial t^2} + \frac{\alpha_{loss}}{2}a_y = j\gamma_{nl}\left(|a_y|^2 + \frac{2}{3}|a_x|^2\right)a_y, \tag{3}$$

and they contain the influences of CD, PMD of 1st and 2nd order as well as the Kerr nonlinearities SPM and PM-XPM. The expressions a_i in (2) and (3) represent $a_i(t,z)$ with $i \in \{x,y\}$ and are the lowpass equivalents of the guided wave at time t and position z in the fiber. α_{loss} is the loss of the fiber. β_{1i} and β_{2i} are the fiber propagation constants and γ_{nl} controlls the Kerr nonlinearity. In the following it is assumed, that the fiber loss α_{loss} is fully compensated by the optical amplifier attenuation G. Therefore α_{loss} and G are neglected.

The transmission of the signal $\overrightarrow{s(t)}$ over the fiber is represented in Fig. 2(b) by the nonlinear operator $\underline{\overrightarrow{b[\cdot]}}$ with memory and the fiber output signal is

$$\overrightarrow{u(t)} = \underline{\overrightarrow{b\left[\overrightarrow{s(t)}\right]}}. \tag{4}$$

After amplification, optical filtering $\overline{\overline{h_o(t)}}$, photo detection $\|\cdot\|_2^2$ and electrical filtering $h_{el}(t)$, the analog

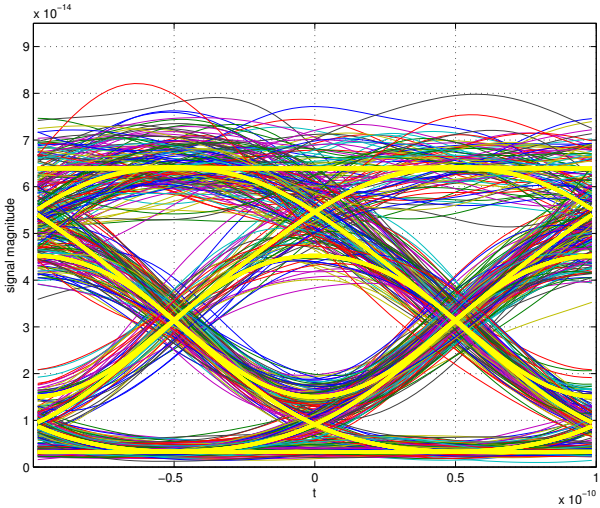

Fig. 3. Noisy (multi color, thin line) and noiseless (yellow, bold line) eye diagram at $E_b/N_o = 20\,\text{dB}$ for the uncoded transmission at $R_b = 10\,\text{Gbit/s}$ and $\Delta\tau = 60ps$ and $R_D = 400ps/nm$.

receive signal can be written as

$$q(t) = \frac{1}{2}\eta\left\|\overline{\overline{h_o(t)}} * \left(\underline{\overrightarrow{b\left[\overrightarrow{s(t)}\right]}} + \overrightarrow{n(t)}\right)\right\|_2^2 * h_{el}(t). \tag{5}$$

In this equation, η is the optoelectronic conversion factor and $\frac{1}{2}$ occurs during the derivation of the equivalent lowpass model. $\overrightarrow{n(t)}$ is the two dimensional complex valued Gaussian noise process, that models the noise of the preamplifier. The polarization components are uncorrelated and the autocorrelation function for x and y direction are $R_{xx}(\tau) = N_{o,pol}$ and $R_{yy}(\tau) = N_{o,pol}$. The receive signal $q(t)$ is plotted in Fig. 3 for the system parameters that are given in Sec. 4. After sampling of $q(t)$ at equidistant sampling instances the signal can then be written as

$$q_m = q(mT_s - t_o), \tag{6}$$

where m is the index of a_m, $T_s = 1/R_s$ is the symbol duration and t_o is simply an arbitrary time shift for synchronization reasons.

3.1.1 The signal to noise ratio definition

The SNR is defined as the ratio of symbol energy E_s to the noise energy N_o in front of the optical filter. The SNR that is applied for a fair FEC code comparison is then defined as the bit energy E_b to the noise energy N_o and

$$\frac{E_b}{N_0} = \frac{E_s}{N_0}\frac{1}{R_c} = \frac{\frac{1}{2}P_{cw}dT_s}{2N_{0,pol}}\frac{1}{R_c} \tag{7}$$

is obtained. $N(f) = N_0$ is the the total noise spectral density of the two dimensional noise process $\overrightarrow{n(t)}$, d is the duty cycle of the impulse shaper, T_s a symbol period and R_c the code rate. The relation to the optical signal to noise ratio (OSNR) is

$$OSNR_{B,dB} = \left.\frac{P_{\text{mean}}}{P_{\text{noise},B}}\right|_{dB} = \left.\frac{E_b}{N_0}\right|_{dB} - 10\log\frac{B}{R_s}\frac{1}{R_c}, \tag{8}$$

where B is the reference bandwidth that is most often chosen to be 12.5 GHz.

3.2 Analytical Branch Metric Computation

After the introduction of the system model in the previous section, this section deals with the analytical evaluation of the PDFs of the samples q_m, according to (6). The PDFs are necessary as branch metrics for the BCJR and Viterbi algorithm. Since the noise properties of the samples q_m are signal dependent, the PDFs have to be evaluated in dependence on a signal state and transition that are defined by the last Q transmitted symbols a_m. The state transition can be described by (s_{m-1}, a_m), where s_{m-1} is the current state of the signal and a_m the current fiber input symbol. In order to derive the PDFs of the samples q_m the sampling instant t_s is introduced and

$$q(t_s) = \frac{1}{2}\eta\left(\int_{-\infty}^{\infty} h_{el}(t_s-\tau)\left|a_x(\tau)+b_x(\tau)\right|^2 d\tau + \int_{-\infty}^{\infty} h_{el}(t_s-\tau)\left|a_y(\tau)+b_y(\tau)\right|^2 d\tau\right), \tag{9}$$

can be written. (9) is obtained after inserting the following expression for the signal in front of the photo diode into (5)

$$\overrightarrow{z(t)} = \overline{\overline{h_o(t)}} * \overrightarrow{y(t)} = \underbrace{\overrightarrow{a(t)}}_{\text{filtered signal}} + \underbrace{\overrightarrow{b(t)}}_{\text{filtered noise}}. \tag{10}$$

In this expression signal and noise are separated from each other.

In order to evaluate the PDF at t_s, the Karhunen-Loève series expansion (KLSE) has to be applied to (9). If a MGF calculus is further applied to the result of the KLSE, the PDF at t_s can be evaluated. This has to be done for each possible state transition (s_{m-1}, a_m). A more detailed description is given in the following.

3.2.1 The Karhunen-Loève Expansion

The KLSE is an orthogonal series expansions for random processes. It can be used to transform a correlated and time continuous random process into an uncorrelated random process. This KLSE is applied to the signals $a_{x,y}(t)$ and the noise components $b_{x,y}(t)$ in (9). Using the resulting discrete representation of $q(t_s)$ the PDF can be calculated by use of a MGF calculus.

The series expansion of the filtered noise components (colored Gaussian noise) in (9) can be written as

$$b_x(t) = \sum_{i=1}^{\infty} u_i f_i(t), \quad b_y(t) = \sum_{i=1}^{\infty} v_i g_i(t) \tag{11}$$

for x and y polarization direction. The sets $\{f_i(t)\}$ and $\{g_i(t)\}$ as well as the sets $\{u_i\}$ and $\{v_i\}$ stand for the orthonormal base functions and the orthogonal coefficients, respectively. The solution of the series expansion is exemparily considered in the following for the x polarization direction, the solution for the y direction is similar.

If the KLSE is applied, then the set of base functions $\{f_i(t)\}$ has to be orthonormal with respect to the weighting function $h_{el}(t_s - t)$ and has to fulfill the orthonormality condition

$$\int_{-\infty}^{\infty} h_{el}(t_s-t)\, f_i(t) f_j^*(t) dt = \delta_{i-j}. \tag{12}$$

The expansion coefficients u_i can be obtained by the integral

$$u_i = \int_{-\infty}^{\infty} h_{el}(t_s-t)\, b_x(t) f_j^*(t) dt. \tag{13}$$

The base functions $f_i(t)$ and the variances λ_i of u_i are the solutions of the Fredholm equation of second kind

$$\int_{-\infty}^{\infty} h_{el}(t_s-\tau)\, R_{xx}(t-\tau)\, f_i(\tau)\, d\tau = \lambda_i f_i(t). \tag{14}$$

The sums in (11) range from $i = 1$ to $i = \infty$, however values for large i can be neglected and it is sufficient to consider only the first M coefficients [13]. The vector representation of all M coefficients is $\mathbf{u} = [u_1, \ldots, u_M]$. The u_i can be interpreted as orthogonal random variables and therefore they fulfill the condition $E\left[u_i u_j^*\right] = \lambda_i \delta_{i-j}$, where λ_i is the variance of u_i. After discretizing equation (14) by use of a Gaussian quadrature formula at the time sampling points τ_k and t_m as well as with the weights w_k the matrix formula

$$\mathbf{RWH_{el}F} = \mathbf{F}\underline{\underline{\lambda}} \tag{15}$$

is obtained, where $\mathbf{R}$ is the discretized kernel $R_{xx}(t_m - \tau_k)$ of the integral equation, $\mathbf{W}$ and $\mathbf{H_{el}}$ contain the weights w_k and the discretized weighting function $h_{el}(t_s - \tau_k)$ on the diagonal, respectively. The matrix $\mathbf{F}$ contains the discretized Eigenvectors in the columns and the matrix $\underline{\underline{\lambda}}$ contains the Eigenvalues on the diagonal, it holds $\boldsymbol{\lambda} = diag\{\underline{\underline{\lambda}}\}$.

The series expansion of the signal part can be written similar to (11) as

$$a_x(t) = \sum_{i=1}^{\infty} \alpha_i f_i(t), \quad a_y(t) = \sum_{i=1}^{\infty} \beta_i g_i(t) \tag{16}$$

where the series coefficients are obtained by

$$\alpha_i = \int_{-\infty}^{\infty} h_{el}(t_s - t)\, a_x(t) f_j^*(t) dt. \tag{17}$$

The combination of M coefficients in vector representation is $\boldsymbol{\alpha} = [\alpha_1, \ldots, \alpha_M]$.

A similar derivation for the y polarization delivers the results for the series coefficients of noise $\mathbf{v} = [v_1, \ldots, v_M]$ and signal $\boldsymbol{\beta} = [\beta_1, \ldots, \beta_M]$. The variances $\boldsymbol{\sigma}$ of $\mathbf{v}$ are computed similarly to $\boldsymbol{\lambda}$.

3.2.2 The discrete representation of the sampled received signal $q(t_s)$

Using the series expansions of signal (16) and noise (11) and applying the orthonormality condition (12) eq. (9) can be written as

$$q(t_s) = \frac{1}{2}\eta \sum_{i=1}^{\infty} |\alpha_i + u_i|^2 + |\beta_i + v_i|^2 . \tag{18}$$

Using the combined representation of x and y polarization $\mathbf{z_a} = [\boldsymbol{\alpha} + \mathbf{u}, \boldsymbol{\beta} + \mathbf{v}]$, from eq. (18) follows

$$q(t_s) = \frac{1}{2}\eta\, \mathbf{z_a} \mathbf{z_a^H}. \tag{19}$$

The variances are then represented by $\boldsymbol{\Lambda} = [\Lambda_1, \ldots, \Lambda_{2M}] = [\boldsymbol{\lambda}, \boldsymbol{\sigma}]$.

3.2.3 The moment generation function and the PDF of $q(t_s)$

The moment generation function (MGF) of $q(t_s) = q_a$ is defined as

$$\begin{aligned} M_{q_a}(s) &= E\left[e^{sq_a}\right] = E\left[e^{s\frac{1}{2}\eta \mathbf{z_a} \mathbf{z_a^H}}\right] \\ &= \int \cdots \int_{\mathbf{z_a}} e^{s\frac{1}{2}\eta \mathbf{z_a} \mathbf{z_a^H}} p_{\mathbf{z_a}}(\mathbf{z_a})\, d\mathbf{z_a} \end{aligned} \tag{20}$$

where $p_{\mathbf{z_a}}(\mathbf{z_a})$ is the PDF of the filtered optical signal and noise that is now represented by the uncorrelated RVs $\boldsymbol{\alpha} + \mathbf{u}$ and $\boldsymbol{\beta} + \mathbf{v}$. According to the fact, that Gaussian RVs stay Gaussian after a linear operation (namely the optical filtering, where $\overrightarrow{n(t)}$ is filtered and $b_x(t)$, $b_y(t)$ are obtained), $\mathbf{u}$ and $\mathbf{v}$ are Gaussian RVs and the PDF $p_{\mathbf{z_a}}(\mathbf{z_a})$ is simply the product of $2M$ complex valued one dimensional Gaussian PDFs. Using this, the integrals in (20) can be evaluated and the MGF is

$$M_{q_a}(s) = \prod_{i=1}^{2M} \frac{e^{\frac{s\frac{1}{2}\eta |\mu_{a,i}|^2}{1 - s\frac{1}{2}\eta\Lambda_i}}}{1 - s\frac{1}{2}\eta\Lambda_i} \tag{21}$$

$$ROC: -\infty < Re\{s\} < \frac{2}{\eta} \min \frac{1}{\Lambda_i} \tag{22}$$

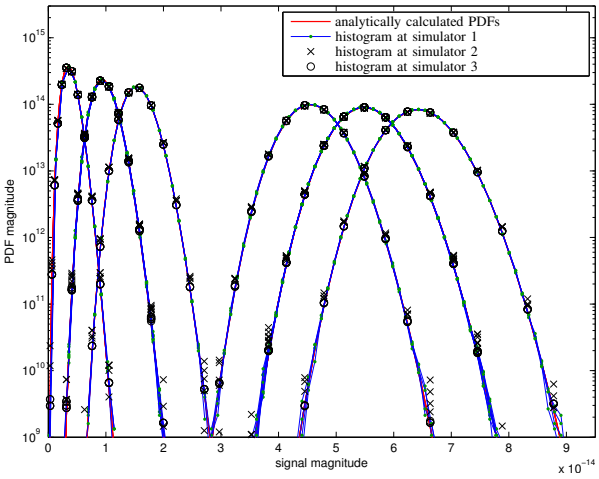

Fig. 4. PDFs for all state transitions (s_{m-1}, a_m) that are necessary to characterize the sampled receive signal fully for $E_b/N_o = 20\,\text{dB}$ and $\Delta\tau = 60ps$ and $R_D = 400ps/nm$.

where ROC is the region of convergence and $Re\{s\} = \sigma'$. The PDF of $q(t_s)$ can then be calculated as

$$p(q_a | s_{m-1}, a_m) = \frac{1}{2\pi j} \int_{\sigma' - j\infty}^{\sigma' + j\infty} M_{q_a}(s)\, e^{-sq_a} dp \tag{23}$$

and the branch metrics, that are necessary for the BCJR and the Viterbi equalizer are found. They are shown in Fig. 4 for the system parameters given in Sec. 4.

4 Performance Analysis and EXIT Chart Discussion

In this section the BER as well as the EXIT chart are discussed, based on a numerical investigation. A computer simulation program that is based on the system model in Sec. 3.1, is used. The system parameters for the discussion are: the net bit rate is $R_b = 10\,\text{Gbit/s}$, the code rate is $R_c = 0.937$. Intensity modulated impulses of non-return-to-zero (NRZ) type with raised cosine impulse shapes and roll off factor $\alpha = 0.35$ are used. The CW TX power is $P_{cw} = 3\,\text{dBm}$, the extinction ratio $\gamma = 13\,\text{dB}$ and the input polarization of the transmitted wave is $\alpha_{pol} = \pi/4$ with respect to the x-polarization direction. The received signal is optically preamplified with an EDFA and optically as well as electrically filtered by Gaussian shaped filters. The optical filter 3 dB bandwidth and the electrical filter 3 dB cut off frequency is $f_{opt,3\,\text{dB}} = 14\,\text{GHz}$ and $f_{el,3\,\text{dB}} = 7\,\text{GHz}$, respectively. The filter bandwidths are optimized using the bandwidth map in Fig. 5. The optoelectronic conversion factor is $\eta = 1$.

Two cases are studied. The first is the back-to-back (BtB) assembly of optical TX and optical RX, where the fiber parameters are as follows: the DGD is $\Delta\tau = 0\,\text{ps}$ and the residual dispersion of the CD is $R_D = 0\,\text{ps/nm}$. The second case is more realistic and exhibits

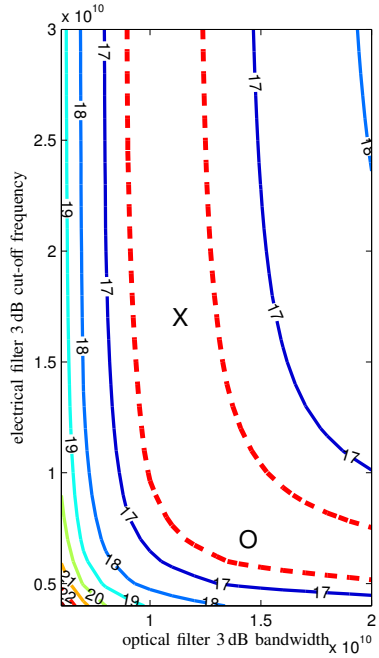

Fig. 5. Receiver filter optimization map. X optimal point, O chosen point. The dashed line marks the area, where the difference to the optimal point is less the 0.2 dB

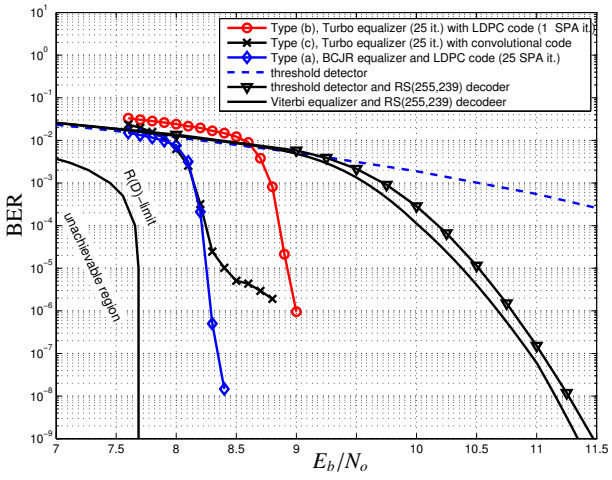

Fig. 6. BER vs. E_b/N_o comparison of different receiver schemes at 10 Gbit/s net bit rate. Back-to-back case, PMD: $\Delta\tau = 0$ ps, CD: $R_D = 0$ ps/nm.

strong PMD and CD. The parameters are $\Delta\tau = 60$ ps and $\Delta\tau = 400$ ps.

4.1 Performance Analysis

The Fig. 6 shows for the BtB case the BER vs. E_b/N_o for a threshold detector, a threshold detector with RS decoder and a RS coded Viterbi equalizer and the three Turbo equalizers under study. Also the rate distortion limit ($R(D)$-limit), which describes the limit of the reachable communication is shown. In Fig. 7, CD and the PMD is introduced. As can be seen, the receiver types (a) and (c) outperform the receiver type (b). The

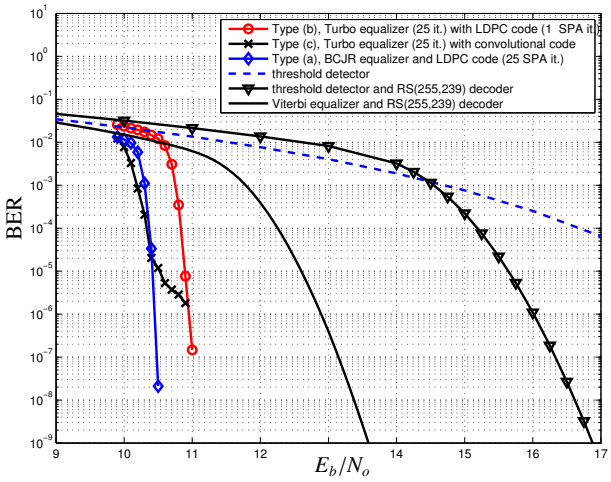

Fig. 7. BER vs. E_b/N_o comparison of different receiver schemes at 10 Gbit/s net bit rate and PMD: $\Delta\tau = 60$ ps, CD: $R_D = 400$ ps/nm.

Turbo cliff of the convolutional coded Turbo equalizer is similar to that of case (a), however, the convolutional coded Turbo equalizer (at least with the parameter settings at hand) develops an error floor at a BER of about 10^{-5} and is therefore out of the race. The winner is this competition is case (a) which is the simplest receiver type. However, further investigations have to be performed especially for the cases if the eye diagram of the received waveforms is closed and much more ISI is present (e.g. for $\Delta\tau > 100$ ps). In the BtB case the gain of the best Turbo equalization method is about 3 dB at a BER of 10^{-9} compared to the RS coded threshold detector and the RS coded Viterbi. The distance to the theoretical limit is about 0.5 dB. For $\Delta\tau = 60$ ps and $\Delta\tau = 400$ ps the gain compared to the RS coded Viterbi equalizer stays 3 dB, however the gain compared to the RS coded threshold detector is more than 6 dB.

A E_b/N_o dispersion penalty can also be extracted from the Figs. 6 and 7. The E_b/N_o penalty of the strong dispersion case to the BtB case is for the type (a) receiver and the RS coded Viterbi equalizer about 2.1 dB and the E_b/N_o penalty of the RS coded threshold detector about 5.5 dB at a BER of 10^{-9}.

4.2 EXIT Chart Discussion

The iterative decoding process of the Turbo equalizers can be analyzed and understood by the EXIT chart. It depicts the iterative decoding at a fixed E_b/N_o. In Fig. 8 the EXIT chart for the convolutional coded Turbo equalizer is shown for 10.1 dB, 10.4 dB and 10.7 dB. In these charts, the equalizer as well as the decoder characteristic is plotted. The decoding trajectory (the decoding path) is also shown. Curves of constant BER are depicted by dotted lines. As can be seen, a decoding tunnel is required to reach low BER in the upper right area of the chart.

The characteristics of equalizer and decoder of the receivers (a), (b) and (c) are given in Fig. 9. The FEC

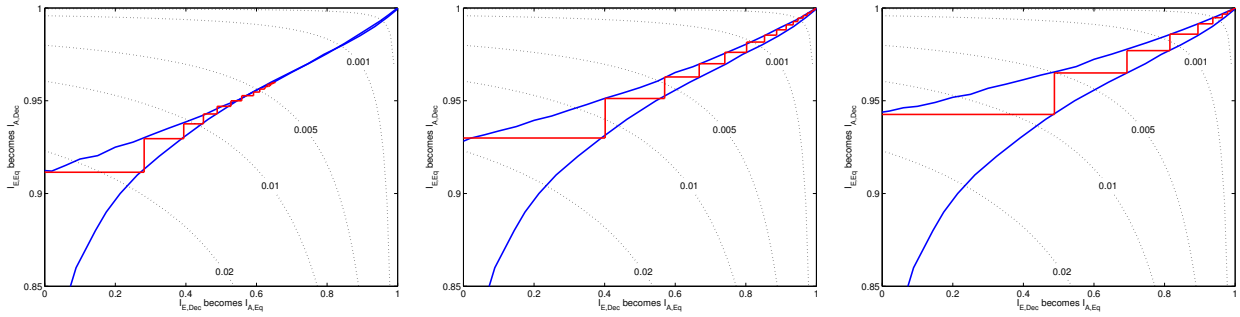

(a) $E_b/N_o = 10.1\,dB$ (b) $E_b/N_o = 10.4\,dB$ (c) $E_b/N_o = 10.7\,dB$

Fig. 8. EXIT charts of the convolutional coded Turbo equalizer at E_b/N_o 10.1 dB, 10.4 dB and 10.7 dB for $\Delta\tau = 60ps$ and $R_D = 400ps/nm$. Decoder characteristic (lower curve), equalizer characteristic (upper curve), trajectory (step curve) and curves of equivalent BER values (dotted).

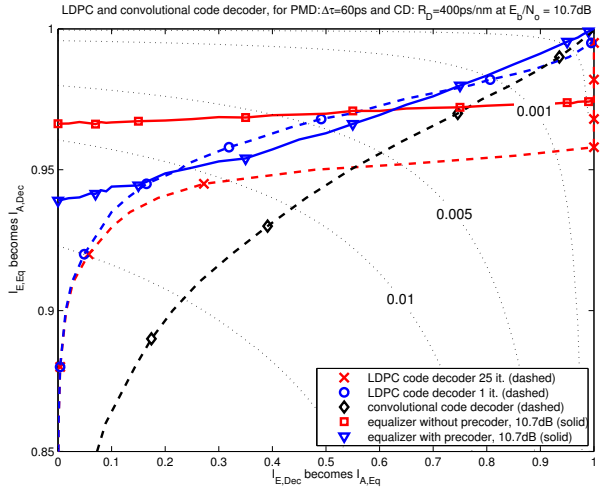

Fig. 9. EXIT chart with comparison of LDPC code and convolutional code based Turbo equalizers.

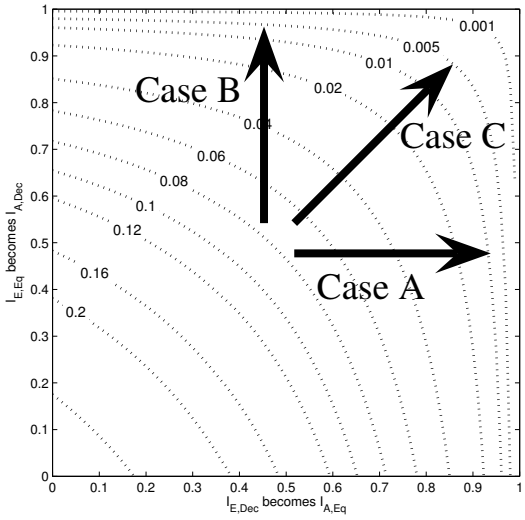

Fig. 10. EXIT chart with the three main cases to reach low bit error rates with Turbo equalization.

decoders (dashed lines) as well as a precoded and a non-precoded BCJR equalizer (solid lines) can be seen. The chart is sketched for 10.7 dB. Obviously, the characteristic of the precoded BCJR reaches the upper right corner of the EXIT chart. Contrary, the scheme without precoder does not reach this point. The non-precoded BCJR has a better (higher) starting point at the left edge of the EXIT diagram. For these equalizers appropriate decoder characteristics have to be found. In case of precoding a convolutional or a LDPC code with a small number of iterations match very well. In the case of a non-precoded system an iterative LDPC code with many iterations is the better choice. With these results, it can be seen, that it is not necessary to reach the upper right corner in the EXIT chart because low BER values can also be reached by forcing the decoders into the regions that are next to the right or the upper boundary of the diagram (see curves of equivalent BER values).

In summary, with the EXIT chart three different cases to reach low BER values can be considered. They are indicated in Fig. 10. The arrows show the direction in which the iterative process has to move.

- **Case A:** Reach the right edge of the EXIT chart. This can be achieved by use of an iterative LDPC decoder in combination with a BCJR equalizer. In this case it is beneficial not to use an precoder, because of the higher starting point of the trajectory at the left edge of the EXIT chart.
- **Case B:** Reach the upper edge of the EXIT chart. In this case the mutual information at the output of the equalizer has to be maximized for $I_A = 0$ (maximize the starting point at the left edge). This can be achieved by increasing the E_b/N_o, which is the trivial case, but it can be also achieved by improving the equalizer.
- **Case C:** Reach the upper right corner $(I_{A,Eq}, I_{A,Dec}) = (1, 1)$. This is the classical Turbo equalization case. The characteristics of equalizer and decoder have to be chosen in a way, that the mentioned point can be reached. This can be achieved by use of a precoder and a proper

decoder characteristic.

- **Generalization:** It is of course possible to combine case A and case C in order to reach low BER values. Then Turbo equalizer and LDPC decoder iterations are used in parallel. However the complexity of the receiver schemes is heavily increased by doing this and the possible gain of this kind of optimization is low, maybe less or around a tenth of a dB (this can be extracted from Fig. 10).

However, optimizations concerning the equalizer and the FEC code will of course increase the system performance of the Turbo equalizer. The general structure of the receiver schemes according to Fig. 1 will however stay the same.

5 Conclusion

In this paper three different Turbo equalizers which are based on two different types of FEC codes are compared, namely convolutional code and LDPC code. The equalizers are further compared to some other types of receivers that are coded by a RS(255,239) code (Viterbi equalizer and threshold detector).

The convolutional coded Turbo equalizer only supports Turbo equalizer iterations. The LDPC coded Turbo equalizer can have two iteration loops, first inside the LDPC decoder and second between equalizer an decoder. This extended parameter set enables it to implement different types of LDPC coded Turbo equalizers.

A BER comparison showed, that the receiver based on a single BCJR pass and 25 LDPC decoder iterations performs well and almost no improvement is achieved by an additional iteration between equalizer and decoder. The convolutional coded Turbo equalizer has about the same Turbo cliff position, however it develops an error floor. The precoded LDPC Turbo equalizer is not a serious option, because the Turbo cliff is far away from the other two solutions. An EXIT chart analysis of the receiver schemes gives detailed insights into the iterative decoding process of the different Turbo equalizers. All the investigations are done based on a sophisticated model of the fiber optic transmission channel and on analytically calculated branch metrics for the BCJR and Viterbi equalizer.

It further turned out, that a large number of combined equalizer and decoder iterations, as it was suggested by [10] provides only a slight gain and that either many LDPC decoder or many Turbo equalizer iterations are preferable.

Finally it can be stated, that a Turbo equalization scheme was found, with a performance, that is only 0.5 dB from the theoretical limit.

References

[1] H. Bülow, F. Buchali, and A. Klekamp, "Electronic dispersion compensation," *JOURNAL OF LIGHTWAVE TECHNOLOGY*, vol. 25, no. 7, pp. 1742–1753, January 2008.

[2] J. H. Winters and S. Kasturia, "Constrained maximum-likelihood detection for high-speed fiber-optic systems," in *Globecom*, 1991, pp. 1574–1579.

[3] J. H. Winters and R. D. Gitlin, "Electrical signal processing techniques in long-haul fiber-optic systems," *IEEE Transactions on Communications*, vol. 38, no. 9, pp. 1439–1453, September 1990.

[4] J. H. Winters, "Equalization in coherent lightwave systems using a fractionally spaced equalizer," *IEEE Journal of Lightwave Technology*, vol. 8, no. 10, pp. 1487–1491, October 1990.

[5] D. Efinger and J. Speidel, "A parallel equalizer for high-speed electronic dispersion compensation," in *European conferenc on optical communications (ECOC)*, 2007.

[6] Y. Cai, J. M. Morris, T. Adalı, , and C. R. Menyuk, "On turbo code decoder performance in optical-fiber communication systems with dominating ASE noise," *Journal of Lightwave Technology*, vol. 21, no. 3, pp. 727–734, March 2003.

[7] R. M. Pyndiah, "Near-optimum decoding of product codes: block turbo codes," *IEEE Transactions on Communications,*, vol. 46, no. 8, pp. 1003–1010, Aug 1998.

[8] I. B. Djordjevic, S. Sankaranarayanan, and B. V. Vasic, "Projective-plane iteratively decodable block codes for wdm high-speed long-haul transmission systems," *IEEE Journal of Lightwave Technology*, vol. 22, no. 3, pp. 695 – 702, March 2003.

[9] M. Jäger, T. Rankl, J. Speidel, F. Buchali, and H. Bülow, "Performance of turbo equalizers for optical PMD channels," *Journal of Lightwave Technology*, vol. 24, no. 3, pp. 1226–1236, March 2006.

[10] I. B. Djordjevic, H. G. Batshon, M. Cvijetic, L. Xu, and T. Wang, "PMD compensation by LDPC-coded turbo equalization," *IEEE Photonics Technology Letters*, vol. 19, no. 15, pp. 1163 – 1165, August 2007.

[11] L. Bahl, J. Cocke, F. Jelinek, and Raviv, "Optimal decoding of linear codes for minimizing symbol error rate," *IEEE Transactions on Information Theory*, vol. 20, no. 2, pp. 284 – 287, March 1977.

[12] T. S. S. of the ITU (ITU-T), *ITU-T Recommendation G.975 - Forward error correction for submarine systems*. International Telecommunications Union (ITU), October 2000.

[13] G. Bosco, A. Carena, V. Curri, R. Gaudino, P. Poggiolini, and S. Benedetto, "A novel analytical approach to the evaluation of the impact of fiber parametric gain on the bit error rate," *IEEE Transactions on Communications*, vol. 49, no. 12, pp. 2154–2163, December 2001.

[14] S. ten Brink, "Convergence of iterative decoding," *IEE Electronics Letters*, vol. 35, no. 10, pp. 806–808, May 1999.

[15] S. Lin and J. Daniel J. Costello, *Error Control Coding*, 2nd ed. New York: Prentice Hall, 2005.

[16] T. S. S. of the ITU (ITU-T), *ITU-T Recommendation G.975.1 - Forward error correction for high bit-rate DWDM submarine systems*. International Telecommunications Union (ITU), February 2004.

[17] P. J. Winzer, M. Pfenningbauer, M. M. Strasser, and W. R. Leeb, "Optimum filter bandwidths for optically preamplified NRZ receivers," *Journal of Lightwave Technology*, vol. 19, no. 9, pp. 1263–1273, September 2001.

[18] G. P. Agrawal, *Nonlinear fiber optics*. Academic Press, 1998.